Case Studies in Chemical and Environmental Engineering 9 (2024) 100620

Contents lists available at ScienceDirect

Case Studies in Chemical and Environmental Engineering

journal homepage: www.sciencedirect.com/journal/case-studies-in-chemical-and-environmental-engineering

Case Report

Effect of polyvinylidene fluoride concentration in PVDF-TiO_2-PVP composite membranes properties and its performance in bovine serum albumin rejection

Rianyza Gayatri [a,b], Ahmad Noor Syimir Fizal [c], Erna Yuliwati [d], Muhamad Zulhilmi Zailani [e], Juhana Jaafar [e], Md Sohrab Hossain [f], Muzafar Zulkifli [g], Wirach Taweepreda [a,**], Ahmad Naim Ahmad Yahaya [g,*]

[a] Polymer Science Program, Division of Physical Science, Faculty of Science, Prince of Songkla University, Hat-Yai, Songkhla, 90110, Thailand
[b] Universiti Kuala Lumpur Malaysian Institute of Chemical and Bioengineering Technology, Alor Gajah, Melaka, 78000, Malaysia
[c] Centre for Sustainability of Ecosystem & Earth Resources (Pusat ALAM) Universiti Malaysia Pahang, Lebuh Persiaran Tun Khalil Yaakob, 26300, Gambang, Pahang, Malaysia
[d] Program Study of Chemical Engineering, Faculty of Engineering, Universitas Muhammadiyah Palembang, Jalan A.Yani 13 Ulu Kota, Palembang, 30263, Indonesia
[e] Advanced Membrane Technology Research Centre (AMTEC), Faculty of Chemical and Energy Engineering, Universiti Teknologi Malaysia, 81310, Skudai, Johor, Malaysia
[f] HICoE-Centre for Biofuel and Biochemical Research, Institute of Self-Sustainable Building, Department of Fundamental and Applied Sciences, Universiti Teknologi PETRONAS, Seri Iskandar, 32610, Perak Darul Ridzuan, Malaysia
[g] Green Chemistry and Sustainability Cluster, Universiti Kuala Lumpur, Branch Campus Malaysian Institute of Chemical and BioEngineering Technology, 78000, Alor Gajah, Melaka, Malaysia

ARTICLE INFO

Keywords:
Polymeric composite
Flat sheet
Composite membrane
Bovine serum albumin rejection
Membrane separation

ABSTRACT

In the present study, the polyvinylidene fluoride (PVDF) was incorporated with polyvinylpyrrolidone (PVP) and titanium dioxide (TiO_2) nanoparticles to prepare PVDF-TiO_2-PVP composite membrane for Bovine Serum Albumin (BSA) rejection from protein contaminated wastewater. The preparation of PVDF-TiO_2-PVP composite membrane was conducted by a non-solvent phase inversion (NIPS) process with varying PVDF weight percentages ranging from 16 to 19 wt%. The polymer concentration plays a critical role in the formation of composite membranes that is commonly overlooked. The primary goal of this study is to examine how the concentration of polymers affects the process of membrane creation, the ensuing structure, and the properties of these membranes. Presently, there is a restricted comprehension concerning the impact of PVDF polymer concentration in the fabrication of membranes using the NIPS approach, particularly for PVDF-TiO_2-PVP composite membranes. FE-SEM analysis revealed the lowest skin layer thickness and the number of macro-void formations in a PVDF composite membrane were at 16 wt% PVDF, compared to composite membranes over higher PVDF concentrations from 17 to 19 wt%. There were only slight variations in the percentages of individual elements across all PVDF-TiO_2-PVP membranes, yet the values were identical for C, O, F, and Ti. The viscosity was lowest at 16 wt percent PVDF (576.5 MPa s) and greatest at 19 wt percent PVDF (2054.3 MPa s). It showed that 19%wt PVDF viscosity increased fourfold higher than 16%wt. As the concentration of PVDF was increased, a related decrease in the surface porosity of the membrane was observed. The highest hydrophobicity with the contact angle of 79.62° of the composite membranes were detected at 19 wt% of PVDF loading. The maximum water flux (265.43 L/m^2h) and BSA flux (250.31 L/m^2h) were obtained at 19 wt% of PVDF loading. The lowest PVDF concentration of 16 wt% rejected BSA with 91.01 % efficiency. At 19 wt% PVDF, the rejection rate dropped nearly sixfold to 16.34 %.

* Corresponding author.
** Corresponding author.
E-mail addresses: wirach.t@psu.ac.th (W. Taweepreda), ahmadnaim@unikl.edu.my (A.N. Ahmad Yahaya).

https://doi.org/10.1016/j.cscee.2024.100620
Received 1 November 2023; Received in revised form 3 January 2024; Accepted 8 January 2024
Available online 9 January 2024

1. Introduction

The World Health Organization reported that over 2 billion people lived in water-stressed countries in 2021. Water contamination from various sources has emerged as a significant problem worldwide due to these numbers [1,2]. The potential of water resources has thus been increased by developing competent water treatment technologies that reduce the difficulties and worries related to water pollution [1,3,4]. The fast expansion of international industry has made water contamination one of the most significant environmental concerns we face today [5,6]. Water and wastewater treatment [7,8], gas separation [9], processing of food and beverages [10], and enzyme and protein concentration [11] are just some applications of membrane mechanisms. Compared to traditional separation methods, membrane technology allows for more precise regulation of treatment rates and product quality [12,13]. Membrane technologies are widely used because they are easy to implement and manage, extremely scalable, need little in the way of energy, high separation efficiency, and have a well-understood performance mechanism [14–16].

Polyvinylidene fluoride (PVDF), polyacrylonitrile (PAN), polyether sulfone (PES), cellulose acetate (CA), and polysulfone (PSf) are some of the polymers often employed as membrane materials today [17,18]. The high chemical resistance, robust temperature resistance, and ease of manufacture of PVDF make it one of the top membrane materials [19, 20]. Water purification with current membranes is complex due to the weak exchange relationship between permeability, selectivity, and fouling. New generations have been made possible by recent advances in nanotechnology. Composites possess a range of outstanding characteristics, including extended durability, enhanced rigidity, superior tensile strength, effective gas-barrier characteristics, resistance to corrosion, reduced weight, and elevated thermal resistance. These attributes provide composites with a distinct advantage over alternative compounds. Composites are materials made up of a matrix (a continuous phase) and reinforced materials (a dispersed phase) [21].

Utilizing nanocomposites is crucial in water purification, including various applications such as portable water treatment, wastewater desalination, and treatment. These nanocomposites are essential for achieving cost-effective and energy-efficient water-cleaning methods while reducing ecological consequences [21,22]. According to Abu-dief and Hamdan [23], the structural components of nanomaterials range in size from 1 to 100 nm. Nanomaterials exhibit distinct mechanical, electrical, optical, and magnetic characteristics compared to conventional materials, owing to their reduced dimensions and increased specific surface area [24–26]. Fouling reduction, improved membrane performance, and extended service life are all possible results of incorporating nanomaterials into the polymer matrix [27]. These nanofillers have improved the membranes in several ways, including increasing their hydrophilicity, reducing pollutant and foulant accumulation, enhancing rejection efficiency, and improving mechanical and thermal characteristics [28–30].

The utilization of titanium dioxide (TiO_2) nanoparticles has been extensively employed in enhancing the efficacy of various membrane processes such as Reverse Osmosis (RO), nanofiltration (NF), ultrafiltration (UF), membrane distillation (MD), pervaporation, and Forward Osmosis (FO). This is primarily attributed to these nanoparticles' exceptional hydrophilicity, favorable antifouling characteristics, remarkable chemical stability, and commendable photochemical reactivity [15,31,32]. As one of the most powerful oxidants, the hydroxyl radical degrades hazardous and poisonous contaminants, pure TiO_2 has found widespread application in water treatment [33]. TiO_2 nanoparticles, polymers, solvents, and other additives form a dope solution for membrane casting and immersion precipitation in the non-solvent-induced phase separation (NIPS) wet process [29]. Organic and inorganic additives improved nanocomposite membranes for stable oil-water emulsion separation. Polyvinylpyrrolidone (PVP) is preferred above other organic additions, according to a literature review, because of its high pore formation efficiency and broad molecular weight (Mw) distribution. Several prior studies have examined the efficacy of PVP as an additive to improve the water permeability of pure membranes fabricated from a variety of polymeric materials [34–36].

Inorganic-organic hybrid membranes have superior performance to their conventional counterparts in various aspects, including hydrophilicity, permeability, separation efficiency, proton conductivity, chemical stability, and mechanical strength [37]. A hydrophilic substance would increase the membrane's hydrophilicity [38]. These enhancements often originate from the nanoparticles themselves. Nanomaterials have been added to polymeric membranes in several studies to boost membrane performance as a whole [39]. The incorporation of TiO_2 into the membrane substrate, similar to the inclusion of multi-walled carbon nanotubes (MWCNTs) and graphene oxide (GO), led to the development of elongated finger-shaped pores. This modification resulted in improved hydrophilicity and porosity [40]. Since TiO_2 nanoparticles agglomerated inside pores and lowered pure water flux, researchers discovered that 20–25 wt% produced the best membrane permeability and hydrophilicity [41]. Antimicrobial nanocomposite membranes incorporating silver nanoparticles have been widely used in recent years [42]. Researchers also discovered that water permeability might be improved by including porous nanoparticles like zeolites in nanocomposite membranes [43].

One of the most significant parameters found to alter those membrane properties is the concentration of polymer in the dope solution [44]. The rationale behind this phenomenon is to form a denser skin layer with increased selectivity when the concentration of polymers in the dope solution is elevated [45]. High permeability properties are desired for an asymmetric membrane with a hyper-thin skin layer [46]. In this study, four different polymer concentrations ranging from 16 to 19 wt% were tested to see how they affected the morphological and mechanical properties of the membrane. PVDF-TiO_2-PVP composite membranes are made by mixing polymeric additions of PVP and nanoparticle TiO_2 in a PVDF polymer solution to boost the membrane's hydrophilicity. A further drawback of blending with high polymeric additive concentrations is that membrane top and bottom structures grow denser. This research investigated the effects of varying the polymer concentration used to create the membrane to increase the PVDF membrane's hydrophilicity.

The polymer concentration is crucial in creating composite membranes using non-solvent phase inversion (NIPS), which is often overlooked. Variations in polymer concentration during membrane preparation can impact the final membrane's structure and performance. Determining the optimal concentration of the polymer to enhance membranes' performances in the separation business is crucial because it will affect the membranes' selectivity and permeability. This work aims to investigate the impact of polymer concentration on the process of membrane formation, the resulting structure, and the properties of these membranes. Currently, there is limited understanding regarding the influence of PVDF polymer concentration in the preparation of membranes using the NIPS method, specifically for PVDF-TiO_2-PVP composite membranes. This study has been conducted to create a PVDF-TiO_2-PVP composite membrane for Bovine Serum Album (BSA) rejection and to investigate the impact of PVDF concentration on membrane characteristics. The PVDF-TiO_2-PVP membrane not only has high hydrophilicity but also good mechanical strength. This broad range of potential uses makes it a highly adaptable material.

2. Experimental method

2.1. Materials

Arkema Inc., in Philadelphia, USA was the source for the PVDF (Kynar®760) (MW: 263000 and polydispersity index (PDI): 2.5). Merck provided n-N-dimethylacetamide (DMAc, >99 %). Degussa P_{25} titanium dioxide (TiO_2) from Evonik GmbH had an average particle size of 21 nm

(anatase). Polyvinylpyrrolidone (PVP) as a pore-forming agent (PVP40, MW = 40000 g/mol and PDI: 0.51) and Bovine Serum Albumin (BSA) (MW = 66000 g/mol) were procured from by Sigma-Aldrich.

2.2. Flat sheet membrane preparation

The non-solvent phase inversion (NIPS) technique was utilized to produce flat sheet membranes. The PVDF pellets were pre-dried (for 24 hours at 50° Celsius), and the dope solution was prepared by dissolving 2 wt% of PVP as an addition to the DMAc solvent and then dispersing 1 % wt.% TiO_2. The solution was heated to 50–60° Celsius and mechanically agitated at 500 rpm to include the PVDF polymer with varying concentrations. After the dope had dissolved entirely, it was placed on an ultrasonicate for 30 minutes to remove any remaining air bubbles. The membrane was immersed in water for 24 hours following the casting process. The membrane air dried at room temperature for about two to three days. Membrane performance was evaluated by monitoring the flux of pure water, the flux of permeate, and the rejection of BSA.

A preliminary investigation also employed a 15 wt% PVDF solution to prepare a dope solution. Nevertheless, the casting process encounters several challenges due to the very liquid nature of the dope solution, resulting in the formation of an inhomogeneous solution. Following the casting process, it has been observed that the flat sheet membrane derived from a 15 % weight PVDF solution is excessively thin. According to Alvi et al. [47], prior research has indicated that membranes containing a lower polymer concentration are hypothesised to possess a more porous structure. Lai et al. [48] also using 15 % PVDF that resulted in the lowest stress values. Hence, the lowest concentration of PVDF that was deemed suitable for investigation in this research was established at 16 wt percent (wt%). The various concentrations of PVDF polymer used in the dope solution are listed in Table 1.

2.3. Membrane characterizations

The viscosity of the membrane dope solution was evaluated using a Modular Compact Rheometer (MCR 302). Energy Dispersive X-Ray (EDX) was used to identify the surface components of the membranes, while a Field Electron Scanning Electron Microscope (FESEM) was used to study the membrane morphology (cross section) at different magnifications. Fourier Transform Infrared Spectroscopy (FTIR) results can show how the functional groups and elements in polymers have changed. The membrane's wettability was measured using a contact angle meter (Drop Meter A-100 contact angle).

The tensile test was performed with LLOYD-LR30K Plus equipment. In the NEXYGEN Plus software, the tensile stress (in Kpa), elongation at break (in percent), and elastic modulus (in MPa) were determined to assess the material's tensile properties. Each membrane was subjected to an average of five measurements. The stroke velocity was recorded at a rate of 50 mm per minute, while the width of the specimen measured 20 mm. The length of the specimen within the gauge section was determined to be 100 mm. Asymmetric porous membranes' porosity and average pore radius were calculated. The membrane's dry-to-wet weight ratio was used to calculate its permeability. The equation (1) provided was utilized to ascertain the porosity of the membrane [49]:

$$\in = \frac{\frac{(w1-w2)}{\rho w}}{\frac{(w1-w2)}{\rho w} + \frac{(w2)}{\rho p}} \text{ x } 100 \quad (1)$$

Table 1
Dope solutions for flat-sheet membranes.

PVDF (%.wt)	TiO_2 (%.wt)	PVP (%.wt)	DMAc(%.wt)
16	1	2	81
17	1	2	80
18	1	2	79
19	1	2	78

Following a 24-h immersion in water, five 1 cm^2 flat sheet membranes were chosen to prepare wet and dry membranes. In this context, the symbol $\in$ represents the porosity of the membrane expressed as a percentage, w_1 denotes the weight of the wet membrane in grams (g), w_2 signifies the importance of the dry membrane in grams (g), ρp corresponds to the density of the polymer in grams per cubic centimeter (g/cm^3), and ρw represents the density of water in grams per cubic centimeter (g/cm^3). Any leftover water on the membranes inside surfaces was removed before weighing. The membranes were weighed after 12 hours of vacuum oven drying at 50 °C.

2.4. Filtration experiment (permeation flux and rejection measurement)

The membrane equipment scheme for flat sheet membrane separation is provided in prior work by Gayatri et al. [19] as a schematic diagram. The water flux was determined by quantifying the volume of water that permeated through the membrane during each specified time interval. The assessment of the membrane's performance was conducted by measuring the flux of pure water. The fraction of BSA rejected by the membrane was used to calculate BSA rejection. The membranes filter a protein solution containing bovine serum albumin (1 g BSA protein/1 L RO water). Experiments with filtration were conducted at 1 bar for 1 hour. The rejection percentage was determined by measuring the concentration in a vial using a spectrophotometer once every 15 minutes for an hour. The calculation of the membrane water flux (J) was performed using Equation (2):

$$J = \frac{Q}{A \text{ x } t} \quad (2)$$

Where J denotes the flux (L/m^2h), Q is the permeate volume (L), t is the required time (h), and A is the effective membrane area (m^2) [47]. To calculate membrane rejection, the following equation (2) was used:

$$R = 1 - \frac{Cp}{Cf} \times 100 \quad (3)$$

The variables Cp and Cf represent the concentrations of BSA in the permeate and feed, respectively, measured in parts per million (ppm). The variable R denotes the rejection percentage. The concentration of BSA in both the permeate and feed was determined by a UV-Vis spectrophotometer, with the maximum absorption wavelength set at 279 nm.

3. Result and discussion

3.1. Membrane characterizations

3.1.1. Viscosity of Membrane's dope solution

The concentration of PVDF in membrane dope solution has a substantial impact on the solution's viscosity. Viscosities of dope solutions of varying PVDF concentrations, as determined by this work, are shown in Table 2. At 16 wt percent PVDF, the viscosity is the least one (only about 576.5 MPa s), while the 19-wt percent PVDF gave the highest viscosity (2054.3 MPa s). It demonstrates that viscosity of 19%wt PVDF increased by fourfold more than that of PVDF concentrations of 16%wt. The solution becomes more viscous when PVDF concentration rises from 16 to 19 wt%. This is because PVDF is a polymer with a high molecular

Table 2
The viscosity of membrane dope as a function of PVDF polymer concentration.

PVDF Concentration (%.wt)	Viscosity (MPa.s)
16	576.5
17	622.71
18	1295.1
19	2054.3

weight, and as the concentration of polymer molecules increases, the solution gets more viscous. The bulk polymer nanocomposite dope solutions had no apparent particles and were mechanically mixed and dispersed homogeneously. Suppressing macro voids requires a material with a high viscosity. Macro voids are reduced when viscosity increases [27]. The solution's viscosity must be high enough to prevent big pores from forming but low enough to allow the solution to be spun into a thin film. The greater viscosity of the solutions may have resulted from the entanglement of the PVDF and pore-forming agent chains [50]. According to previous research, adding TiO_2 increased the viscosity of a 16 wt% PVDF membrane to 1789 MPa s, and adding PVP enhanced it to 1992 MPa s [19].

In a study carried out by Nabian et al. [51], it was observed that the PSf-18 membrane exhibited a sponge-like structure as a consequence of the elevated polymer concentration. This rise in polymer concentration led to an augmented viscosity of the polymer, hence causing a delay in phase separation and the subsequent formation of smaller pore sizes. It was also found by Ismail et al. [46] that PSf/NMP solution viscosity rose with PSf content. The entanglement of polymer chains is likely to blame for this unexpected increase in viscosity. Membranes with a sponge-like structure were reportedly created when the viscosity of the polymer dopes was increased [52].

Dope solution viscosity increases due to increased interaction between polymer dope components (thermal effect). It is well established that the sum of these influences significantly impacted the development of the membrane structure [53]. Non-solvent additions in dope solution decrease system miscibility and increase phase inversion rate. Dope solution viscosity impacts phase separation rate [54]. This crucial parameter impacts solvent-non-solvent diffusion and phase inversion kinetics [55]. The viscosity of the polymeric solution is crucial in determining the final shape of the membranes when creating membranes [56]. The viscosity of the solution increases as the polymer concentration increases because the polymer molecules become more entangled with one another, making the solution flow more difficult. The longer the polymer must establish up its network structure before the solvent evaporates, the more viscous the solution [46]. As a result, membranes with more uniform pore size are possible. Casting a solution onto a support membrane might be difficult if the solution is viscous. This could lead to the formation of faulty membranes.

Both academia and industry are interested in miscible polymer mixes. Without particular interactions, polymers are immiscible. Copolymer–copolymer or copolymer–homopolymer blends often form miscible systems without specific interactions. This copolymer effect in polymer blends is explained by mean-field theory. Even without specific interactions between polymer segments, such blends mix exothermically [57].

The thermodynamic compatibility between PVDF (Polyvinylidene fluoride), PVP (Polyvinylpyrrolidone), and TiO_2 nanoparticles in mixed matrix membranes is a critical aspect that influences their structural stability, dispersion, and overall performance. PVDF and PVP are chemically distinct polymers. The compatibility between them depends on the nature of their interactions. While PVDF is a semi-crystalline polymer with a high degree of electronegativity, PVP is amorphous and possesses polar groups, enhancing its hydrophilicity. Thermodynamically, the introduction of TiO_2 NPs into the PVDF matrix alters the system's free energy, impacting the overall stability and properties of the composite. Compatibility is influenced by the intermolecular forces, leading to changes in the composite's mechanical, thermal, and transport properties.

Due to a negligible combinatorial entropy increase in high polymer mixes, the heat of mixing governs polymer-polymer miscibility. An exothermic mixing exceeds the negative equation-of-state effect on mixing thermodynamics. Thus, miscible polymer blends occur when components interact. Polymer blend miscibility is somewhat associated with small molecular weight compound mixing heat [58].

Polymer mixtures have a low entropy of mixing per unit volume compared to small molecule mixtures because they involve fewer molecules. For systems with exothermic mixing heat, homogeneous polymer blends result [59]. The strong repulsive interaction between monomer residues in the copolymer and the homopolymer is diluted by the latter, making the former less repellent [60].

3.1.2. FESEM-EDX of membranes

The cross-sectional morphology of the PVDF-TiO_2-PVP membranes with various PVDF polymer concentrations at a magnification of 600 is illustrated in Fig. 1. FESEM pictures showed that the finger-like structure in PVDF widened over time across the membrane's cross-section. The finger-like structure in the FESEM pictures indicates that all membranes are asymmetric. PVDF pristine demonstrated that TiO_2 added to the membrane structure made it more porous. As shown in Fig. 1b, the membrane structure becomes slightly more porous when TiO_2 is added to the PVDF in its pure form (Fig. 1a). Larger pores on the membrane matrix result from adding TiO_2 nanofillers to a membrane dope [3]. It was discovered that while TiO_2 nanoparticles were widely distributed over membrane surfaces, they tended to clump together into larger aggregates. Although there appeared to be more pores in the membrane at higher TiO_2 concentrations, the agglomerated nanoparticles of TiO_2 would have blocked the pores, reducing water flux [61]. Incorporating TiO_2 loading enlarges the finger-like pores of the enhanced membranes [62].

The macro voids in the membrane modified with PVP are more significant than those in the pure PVDF-TiO_2 membrane, as was observed membrane [63]. One way polymer concentration affects the morphological aspects of an asymmetric membrane is by creating a thicker skin layer and the growth of macro-void structures in the porous substructure [46]. High concentration PVDF membranes have smaller pores and a more consistent pore size distribution. At increasing concentrations, PVDF chains form a denser network, which prevents bigger pores. At lower concentrations, PVDF chains are less densely packed, allowing bigger pores. FE-SEM images (Fig. 1 c-f) demonstrate that varying concentrations of PVDF produce distinct outcomes; a membrane made from 16 wt% of PVDF displays a thinner skin layer and a more significant presence of macro-voids than one earned from PVDF with a higher concentration (17–19 wt%). The results are consistent with those of another study that found the higher the polymer concentration in the dope solution, the denser the skin layer and the smaller the resulting macro-void structure. Finger-like or sponge-like structures made of PVP are commonly used to increase water flux through membranes [61].

As presented in FESEM analysis (Fig. 1), the thickness of pure PVDF is lower (60.48–62.50 μm) than the composite membrane, while that of PVDF-TiO_2 is 65.11–66.22 μm. Table 3 results further confirm that the concentration of PVDF used affects the thickness of composite membranes. The PVDF-TiO_2-PVP membrane has the smallest thickness in the range of 117.7–123.4 μm when 16 wt% of PVDF is present, increases to 234.4–241.8 μm at 17 wt%, and reaches the range of 244.3–246.4 μm at 18 wt%. The uniformity of the dope solution and the hand-casting procedure in flat sheet membrane manufacturing contributed to the modest decrease in thickness value (213.6–214.6 μm) when 19 wt % of PVDF was used. The rapid separation of solvent and non-solvent during phase inversion forms a thin layer on the surface [64].

Extensive finger-like macro-voids form in the porous sublayer due to the higher diffusion rate of non-solvent into the polymer-poor phase compared to the outward diffusion rate of the solvent [65]. Similar research by Abdullah et al. [66] showed that membranes with 20 wt% PES polymer exhibited thicker separation layers, smoother surfaces, and homogenous pores. Compared to PSf-20 and PSf-25, the PSf-30 membrane had the densest skin layer, indicating that increasing polymer concentration in the dope solution decreases macro-void structure [46].

The number of macro-voids decreases as PSf polymer concentration in the dope solution increases, yet their teardrop geometry differs from other membranes. The creation of the PSf-30 membrane's sponge-like shape is also mainly attributable to the dope solution's increased

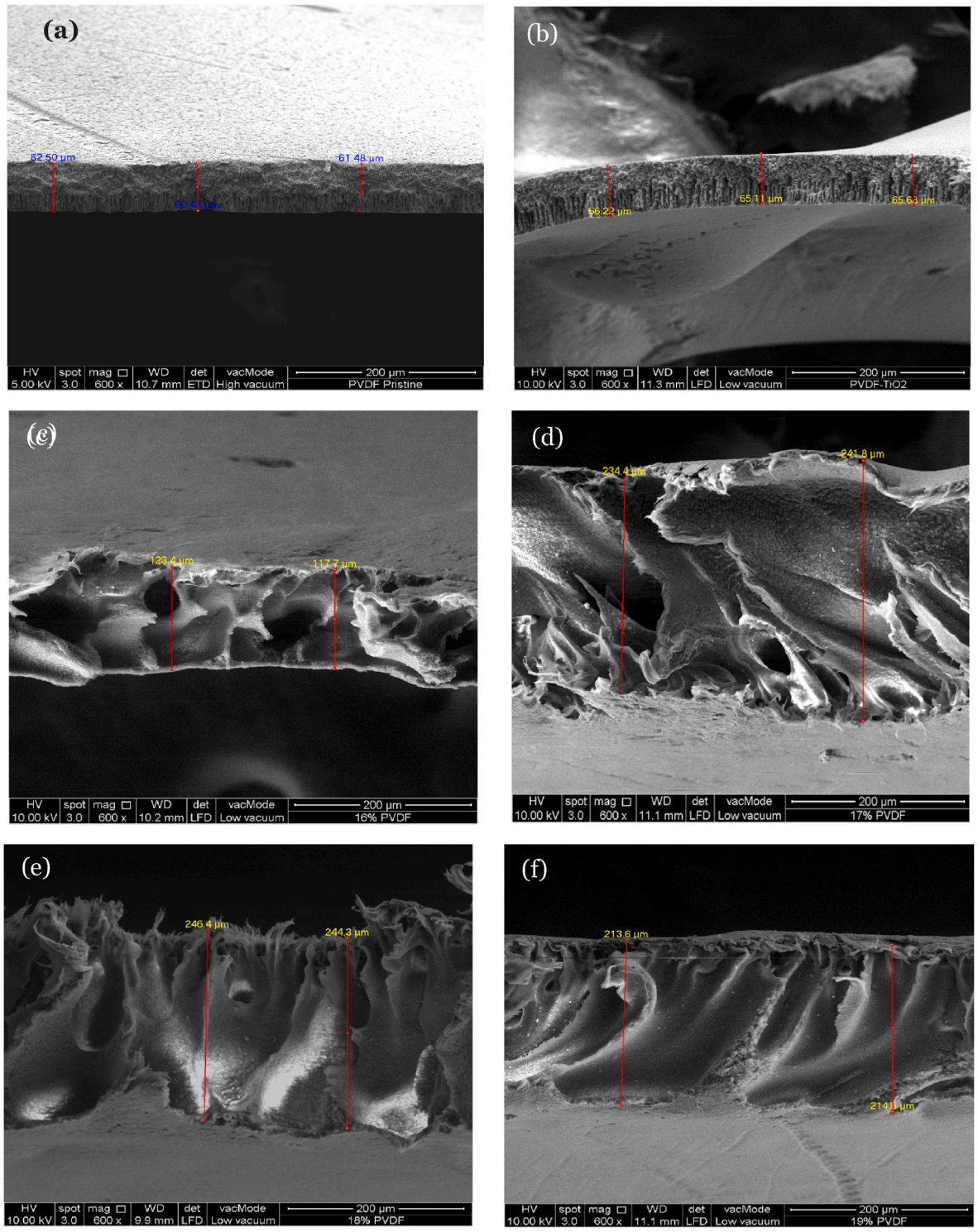

Fig. 1. FE-SEM images (cross-section) of (a) PVDF pristine; b) PVDF-TiO_2; (c) 16 wt% PVDF in PVDF-TiO_2-PVP; (d) 17 wt% PVDF in PVDF-TiO_2-PVP; (e) 18 wt% PVDF in PVDF-TiO_2-PVP; (f) 19 wt% PVDF in PVDF-TiO_2-PVP.

Table 3
The thickness of PVDF composite flat sheet membranes.

PVDF Concentration (wt.%)	Thickness (µm)
16	117.7–123.4
17	234.4–241.8
18	244.3–246.4
19	213.6–214.6

viscosity. According to diffusion exchange kinetics, when the dope solution viscosity increases, the membrane shape becomes sponge-like [44].

Changes in skin layer, bottom layer thickness, and macro void structure show how polymer concentration affects membrane morphology. Polymer concentration raised skin and bottom layer thickness and changed macro-void form from finger-like to teardrop [44]. The EDX data and FESEM images support the successful integration of TiO_2 nanoparticles and PVP into the PVDF membrane. The EDX

results indicate morphological changes, while the FESEM images demonstrate the reduction of finger-like macro voids on the membrane's surface.

Fig. 2 displays the structural arrangement and constituent elements of the produced membranes. The PVDF pristine membrane showed its elemental composition consisting solely of fluorine (F), oxygen (O), and carbon (C). In contrast, the membranes treated with a 1 wt% dose of TiO_2, as depicted in (Figure b), displayed an elemental composition that included carbon (C), oxygen (O), fluorine (F), and titanium (Ti). The Ti element represents the TiO_2 presence in membranes. It proves the successful incorporation of TiO_2 in PVDF membrane. Membranes with different polymer concentration 16 to 19 wt% PVDF dosages (Figure c, d, e, and f), on the other hand shows similar elemental result with all PVDF-TiO_2-PVP membranes (C, O, F, and Ti) with slightly different in weight percentage of each element, as also presented in Table 4. Carbon and florin show the two largest percentages (approximately 50 wt%) in membrane composition due to the large PVDF weight percentage in membrane dope solution, while the titanium weight percentage in all PVDF concentrations is around 2–3%. PVP only acted as a pore former agent during the phase inversion process, so the elements in PVDF-TiO_2-PVP membranes of all PVDF concentrations are identical to those in PVDF-TiO_2 membranes. PVDF-TiO_2 membranes display heterogeneous dispersion and particle fragmentation, increasing dope agglomeration and increasing viscosity [62].

3.1.3. FTIR spectra of membranes

Fig. 3 presents the FTIR spectra of pristine PVDF and PVDF/TiO_2/PVP mixed-matrix membranes. The experimental findings indicate that the detection of PVDF was achieved through the observation of a C–F stretching vibration peak at a wavenumber of 1169.08 cm^{-1} in the PVDF-TiO_2 membrane. The vibrational band observed at a wavenumber of 1402.45 cm^{-1} can be attributed to the deformation vibration of the CH_2 group. Similarly, the presence of a band at 1071.62 cm^{-1} can be attributed to the β crystalline phase of PVDF. The detected peaks at 877.07 and 839.82 cm^{-1} corresponded to the rocking modes shown by the vinylidene group inside the polymer. The observed spectral peaks at a wavenumber of 598.90 cm^{-1} can be attributed to the vibrational modes involving the shaking and bending motion of CF_2 [67]. It is in similar line with the FTIR result obtained from Gayatri et al. [19] showed the peaks observed at 1400 cm^{-1} were associated with the deformation vibration of $–CH_2$. The peaks at 1274 cm^{-1} and 1179 cm^{-1} were also attributed to the symmetrical and asymmetrical stretching of $–CF_2$, respectively. The peak observed at 877 cm^{-1} was identified as one of the characteristic peaks of PVDF. The peak at 840 cm^{-1} was

Table 4
EDX result of PVDF pristine and PVDF composite membranes.

Membranes	Element (Weight%)			
	Carbon	Oxygen	Fluorin	Titanium
PVDF Pristine	52.65	1.03	46.32	0
PVDF-TiO_2	50.29	1.99	45.18	2.54
PVDF-TiO_2-PVP (16 wt% PVDF)	44.03	2.36	51.03	2.59
PVDF-TiO_2-PVP (17 wt% PVDF)	48.75	2.31	45.45	3.50
PVDF-TiO_2-PVP (18 wt% PVDF)	48.68	2.88	45.18	3.27
PVDF-TiO_2-PVP (19 wt% PVDF)	42.24	1.64	52.21	3.90

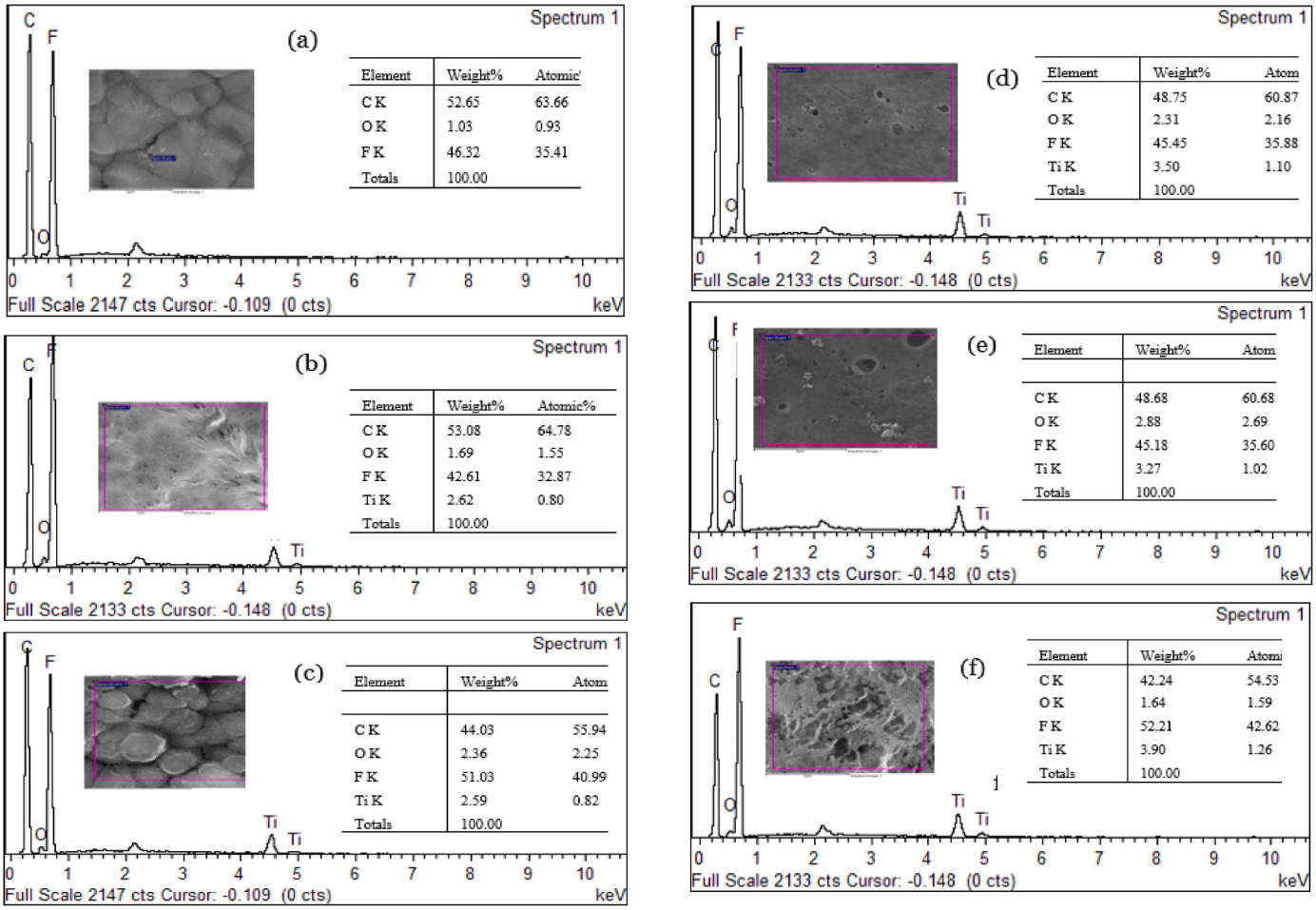

Fig. 2. EDX images of Different Membranes and Different PVDF Concentrations (16–19 wt%). (a) PVDF Pristine Membrane, (b) PVDF-TiO_2 Membrane, (c) 16 wt% in PVDF-TiO_2-PVP Membrane, (d) 17 wt% in PVDF-TiO_2-PVP Membrane, (e) 18 wt% in PVDF-TiO_2-PVP Membrane, and (f) 19 wt% in PVDF-TiO_2-PVP Membrane.

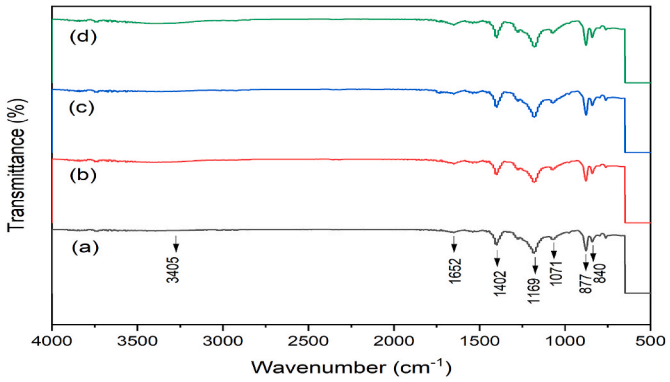

Fig. 3. FTIR Spectra of PVDF-TiO_2-PVP Flatsheet Membranes with Different PVDF Concentrations. (a) 16 wt% PVDF; (b) 17 wt% PVDF; (c) 18 wt% PVDF; (d) 19 wt% PVDF.

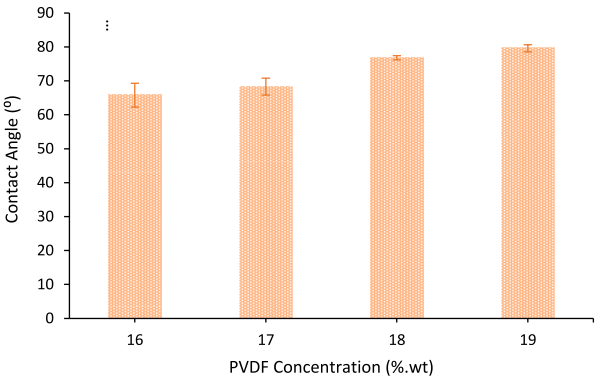

Fig. 4. Contact angle of PVDF-TiO_2-PVP flatsheet membranes with different PVDF concentrations.

determined to be related to the stretching vibration of –CH [68].

Bands between 800 and 1400 cm^{-1} were attributed to lattice vibrations of TiO_2 in the composite, as reported by Rusli et al. [67]. The crystalline phase of PVDF at 762 cm^{-1} peak intensity decreases with increasing concentrations of TiO_2 due to interaction with PVDF. The FTIR measurements determined that the bonding of TiO_2 on the PVDF surface was unaffected by the hot press [67]. The critical peak of TiO_2 remained present at 598.90 cm^{-1}. The –OH stretching vibration is shown by the peak between 1065 and 1070 cm^{-1} [69]. This is due to the presence of hydroxyl groups (-OH) on the surface of the membrane, which can interact with water molecules. According to Abdennouri et al. [70], the band at 3405 cm^{-1} is often attributed to the stretching and bending of the Ti–OH groups' hydroxyl vibration. According to Fadaei et al. [71], an absorption band at 840 cm^{-1} suggested the presence of crystal formations in PVDF membrane. Both PVDF-TiO_2-PVP and PVDF membranes showed a stretching vibrational peak of CO at 1650 cm^{-1} indicating the existence of residues [55]. PVP with a high molecular weight (MW > 10000 g/mol) is more likely to be embedded in the membrane [72]. The stretching vibrations of C–N, C═O, and CH_2 bonds produced three separate peaks in the PVP spectrum at 1290 cm^{-1}, 1660 cm^{-1}, and 1463 cm^{-1}. The presence of these peaks confirms the presence of PVDF, TiO_2, and PVP in the membrane. The peak at 1065–1070 cm^{-1} is particularly interesting, as it indicates that the membrane has a high degree of hydrophilicity.

3.1.4. Contact angle measurement

The effect of PVDF concentration on membrane contact angle has been studied by several researchers. In general, it has been found that increasing the PVDF concentration in the casting solution leads to an increase in the water contact angle of the resulting membrane. The results from Fig. 4 showed that the contact angle was minimal at 16 wt% PVDF (65.79°). Flat sheet membranes made of PVDF-TiO_2-PVP with the highest PVDF concentration (19 wt%) were found to have the biggest contact angles (79.62°). The increasing contact angle value seen during measurement is attributed to the rising polymer concentration in the dope solution. This is because PVDF is a hydrophobic polymer, and as the concentration of PVDF increases, the surface of the membrane becomes more hydrophobic. Naim and Ismail [73] postulate that this trend can be explained by a rise in the proportion of aromatic imide in the polymer's repeating unit, increasing hydrophilicity. A study by Pramono et al. [74] consistent with this discovery, found that increasing the PVDF content made the membranes more hydrophobic (a larger contact angle between the membrane and water). The PVDF membrane at 15 % concentration has the smallest contact angle (64°), indicating the greatest hydrophilicity, whereas the PVDF membrane at 21 % concentration has the largest contact angle (78°). The decreased contact between the membrane and the water can be explained by the hydrophobic characteristic of PVDF which increases with concentration. Reverse osmosis and ultrafiltration can benefit from membranes with larger contact angles since they are less likely to be wetted by water and are less likely to become fouled. The contact angle also increases when the concentration of PVDF increases [75] due to the rougher surface of the membrane. Surface roughness correlates positively with hydrophobicity. Substrate roughness can be altered to make membranes more hydrophobic [76]. The results of these analyses demonstrate a regular pattern in the relationship between PVDF concentration and membrane contact angle.

3.1.5. Membrane porosity

The membrane mass transfer coefficient increases as membrane porosity increases because the solute should permeate through the membrane via the void space of the membrane. It has been observed that the porosity of membranes decreases as the PVDF content rises. This is because PVDF is a hydrophobic polymer, and its compact structure becomes less permeable to water as its concentration increases.

Table 5 demonstrates that as the polymer concentration in the dope solution increased from 16 wt% to 19 wt%, the membrane's porosity and mean pore size decreased. While the porosity of PVDF at 16 % wt was 85.21 %, it was lower at 17 % wt (84.95 %), and it dropped further to 82.44 % and 80.93 % at 18 % wt and 19 % wt, respectively. Consistent with this pattern, Ahmad et al. [54] found that increasing the polymer concentration (from 13 to 19 wt%) significantly reduced the membrane porosity from 70 to 61 %. As the solution viscosity increased, the exchange rate slowed considerably resulting in a more compact membrane structure and less open space as the polymer concentration increased. A study by Nabian et al. [52] found that boosting the PVDF polymer concentration in the dope solution from 16 wt% to 19 wt% reduced the membrane's porosity and mean pore size. The results of these studies suggest that the porosity of PVDF-TiO_2-PVP membranes can be controlled by adjusting the PVDF concentration.

3.1.6. Tensile test

Table 6 displays the results of tensile tests performed on membranes with varying concentrations of PVDF. Measurements of tensile strength and elongation at break are used to analyze the impact of polymer

Table 5
Porosity of PVDF-TiO_2-PVP membranes.

PVDF Concentration (wt.%)	Porosity (%)
16	85.218
17	84.949
18	82.438
19	80.936

Table 6
Tensile properties of PVDF-TiO_2-PVP membranes.

PVDF Concentration (wt.%)	Tensile Strength (KPa)	Elongation at Break (%)	Elastic Modulus (MPa)
16	1.161 ± 0.127	15.031 ± 3.612	14.821 ± 4.891
17	2.219 ± 1.557	11.395 ± 2.234	14.868 ± 4.631
18	2.650 ± 0.049	11.004 ± 3.577	13.618 ± 1.684
19	2.738 ± 0.296	15.827 ± 1.559	16.549 ± 0.539

concentration on the membrane's mechanical properties. The mechanical qualities of a membrane influence how well it can withstand the pressure exerted on it during its various uses [74]. The tensile strength of the membrane improved with increasing PVDF content. This is because a membrane with a higher PVDF content is denser and more compact, making it more resistant to damage. The membrane with 16 wt% PVDF has the lowest tensile strength (1.161 ± 0.127 KPa), whereas the membrane with 19 wt% PVDF has the strongest (2.738 ± 0.296 KPa). The elastic modulus followed the same patterns, with the most significant value recorded at 15.827 MPa for 19 wt% of PVDF. The high value of strain demonstrates the elastic behavior of PVDF membranes [74]. The greater the PVDF concentration, the closer the polymer chains are packed together, making the membrane more rigid, less prone to deformation, and decreasing the elongation at break. Since higher concentrations of PVDF are more resistant to stress, the elastic modulus also rose with increasing concentrations of PVDF.

Others have also reported this finding. The strain in 19 % PVDF is the greatest of any composition studied (148 %), whereas 15 % PVDF has the lowest stress values [77]. The ability to prevent membrane breakage during filtering operations indicates that a membrane's elasticity will contribute to a long service life [74]. The mechanical properties unfortunately are lowered due to the presence of hydrophilic additives [12]. Research by Ismail et al. [46] demonstrate similar tendencies, higher polymer concentration results in excellent membrane tensile strength. Improvements in the membrane's morphological structure are usually responsible for improved tensile strength. Improvements in membrane structure have been seen with increasing polymer concentration [78]. This is because the creation of macro-void systems has decreased and become smaller.

The variation in elongation at break concerning polymer content is also shown. The tensile strength data follows a slightly typical pattern over polymer concentrations. The elongation at break decreased to 11.395 % from 15.031 % when the PVDF concentration is raised from 16 to 17 wt%, then further decreased to 11.004 % at 18 wt% of PVDF concentration, but it raised to 15.827 % at PVDF concentrations of 19 wt %. Consistent with previous research, increasing the polymer concentration from 20 % to 25 wt% initially increased the elongation at break. The elongation at break declines as the polymer concentration approaches 30 wt% in contrast to the tensile strength result. This phenomenon occurred presumably because of the rigidified membrane structure with increasing polymer concentration since elongation at break represents how long the membrane can be stretched before it breaks [46].

The mechanical properties were assessed using the yield stress, elongation at break, and elongation at break as metrics [79]. With increasing density, the elongation at break has marginally increased while the tensile strength at break has slightly decreased [80]. The mechanical properties are significantly influenced by the comonomer concentration, molecular weight, polydispersity index (PDI), and the method of preparation, which governs the uniformity. The melt index (MI) of a polymer is determined by its molecular weight and distribution; generally, as molecular weight increases, MI values decrease [81]. By utilizing compatible polymer mixtures, it is possible to achieve favorable mechanical properties that are comparable to, and occasionally even surpass (via synergistic effect), those achievable with the polymers used as individual components [82].

3.2. Performance evaluation of membranes

3.2.1. Pure water flux and BSA flux measurement

Permeability and selectivity of membranes were evaluated by measuring the flux of pure water and BSA solution. Fig. 5 demonstrates the impact of PVDF concentration on pure water flux across PVDF-TiO_2-PVP membranes. It has been discovered that raising the percentage of PVDF causes a greater flux of pure water. PVDF is a hydrophobic polymer and including it in the membrane matrix makes it harder for water molecules to diffuse across the membrane. At very high concentrations of PVDF, the membrane can become excessively hard and impermeable, limiting the flow of pure water. In accordance with the FESEM result showing that an increase in the polymer concentration in a dope solution theoretically leads to a denser formation of skin layer then a lesser and smaller formation of macro-voids structure, the water flux increased with higher PVDF concentration. The lowest water flux was seen at 16 wt% PVDF (95.84 L/m^2h) and the greatest was at 19 wt% PVDF (265.43 L/m^2h). The water flux was greater for the membranes with a higher PVDF content. These membranes' smaller pore sizes created less friction for water to flow through.

The lowest water flux was observed at 16 wt percent PVDF (95.84 L/m^2h), while the highest was recorded at 19 wt percent PVDF, where it nearly tripled (265.43 L/m^2h) than the least concentration. The water flux was greater for the membranes with a higher PVDF content. As presented in Fig. 5, PVDF concentrations between 16 and 18 wt percent showed no significant increase, while the highest concentration produced the greatest flux. These membranes' smaller pore sizes created less friction for water to flow through.

Similar patterns were seen for BSA flux; the maximum BSA flux (250.31 L/m^2h) was produced by the highest PVDF concentration, while the lowest flux (87.23 L/m^2h), which was nearly three times lower than the highest, was produced by the smallest PVDF concentration. Similar trends were seen for BSA flux; the greatest PVDF concentration resulted in the highest BSA flux (250.31 L/m^2h). The creation of finger-like or sponge-like structures in the membrane sub-layer is often attributed to the improvement in membrane water flux with the addition of PVP. Previous studies by Ong et al. [61] found that increasing the molecular weight (Mw) of PVP significantly suppressed macro void development and resulted in a denser epidermal layer and reducing water flux. Several factors contribute to the high pure water flux of PVDF-TiO_2-PVP membranes. The hydrophilic surface provided by TiO_2 nanoparticles in the membrane promotes interactions between water molecules and the membrane. In addition to facilitating water molecule transport, the PVP polymer in the membrane also leads to a more open pore structure that allows for greater membrane fluidity [19]. Operating factors, such as pressure and temperature, can also influence the membrane's pure water flux. Pure water fluxes tend to increase when pressures and temperatures rise.

Another pattern is shown by Pramono et al. [74] study, which found that a PVDF membrane with a thickness of 15 % produced the maximum water flux while a PVDF membrane with a thickness of 21 % produced the lowest. The flux of pure water through a membrane decreases as its thickness increases because water flow resistance increases. According to the contact angle measurements, the 15 % PVDF membrane is the most polar which explains its high-water flux and powerful interactions with water. This demonstrates that membrane surface and pore characteristics affect membrane permeability and perm-selectivity. Denser membranes result in lower water flows because of their decreased permeability [83]. The pure water flow in PVDF-TiO_2-PVP membranes can be affected by several factors beyond just the PVDF content. The operating pressure, casting temperature, crossflow velocity, and casting solvent plays a role. Producing PVDF-TiO_2-PVP membranes with high pure water flux and strong separation performance requires strict control of these variables. Previous research by Abdullah et al. [66] found that a higher polymer weight percentage (20 % PES) resulted in a more significant dye rejection percentage (67.33 %) and permeate flux

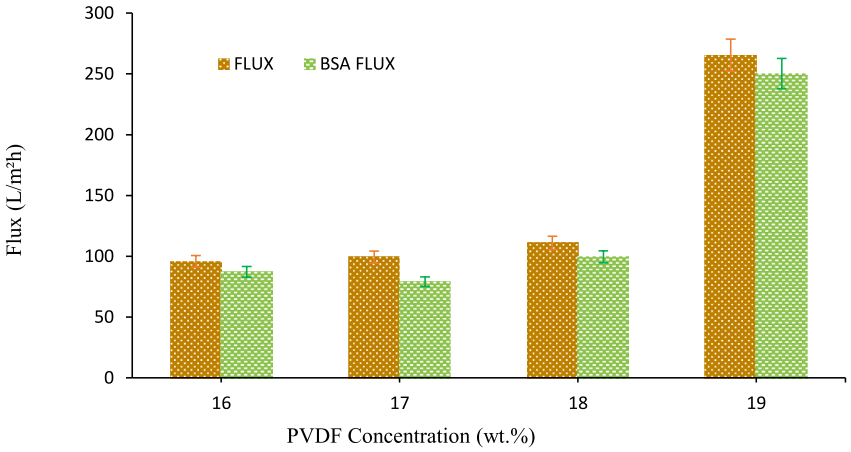

Fig. 5. Pure water flux and BSA flux of Membranes with Different PVDF Concentrations.

(10.024 L/m^{2}h) than a lower polymer weight percentage (16–18 wt%).

3.2.2. BSA rejection test (BSA removal performances)

The BSA removal performances of the prepared membranes are shown in Fig. 6. Fig. 6 demonstrates how dopes with greater PVDF concentrations result in denser membranes and how decreasing BSA rejection was produced as PVDF concentration increased. A concentration of 16 wt percent PVDF results in a BSA rejection of 91.01 % (the highest), whereas a concentration of 19 wt percent PVDF results in the lowest BSA rejection of 16.34 %. The BSA rejection for 17 wt% and 18 wt % PVDF concentration were 89.71 % and 47.42 %, respectively. BSA rejections were reduced in membranes with higher PVDF content. Membranes exhibiting an increased concentration of polyvinylidene fluoride (PVDF) manifest a more homogeneous distribution of pore sizes and exhibit reduced pore dimensions. These less permeable structures generated a significant resistance to protein molecules [84]. This is because the BSA molecules could get through the membranes since the bigger holes gave less barrier to water flow. Results showed that membrane water flux and BSA rejection were enhanced by incorporating TiO_2 into the PVDF matrix. Similar tests by Nabian et al. [52] found that the PSF-16 membrane had lower mass transfer resistance than the PSF-18 membrane. As previously indicated in the discussion of membrane permeability, the investigation shows that pore size and surface characteristics also impact membrane rejection [74].

The accepted view in the scientific community was that a hydrophilic membrane could attract water molecules and create a layer of hydration and steric hindrance on its surface. This phenomenon has been observed to effectively impede the adsorption of proteins, such as Bovine Serum Albumin (BSA), as demonstrated by Wu et al. [85]. The increased rejection of BSA may be attributed to the influence of titanium dioxide (TiO_2) incorporation into the membrane matrices. According to Kumar et al. [86], including TiO_2 nanoparticles increased the negative charge of the produced membranes. This can be attributed to the presence of carboxylic groups, –OH groups, and Ti–OH groups, which exhibit a higher negative charge on the surfaces and matrixes of the membranes. In contrast, it has been observed that when the pH is at 7, which is significantly different from the isoelectric point (IEP) of 4.9 for BSA protein, the protein acquires a more significant negative charge. This increased negative charge is believed to result in a more significant electrostatic repulsion between BSA and the modified membranes, as Mo et al. [87] suggested. However, it is worth noting that specific characteristics of BSA removal can also be explained by protein adsorption onto the membrane surface within this pH range, which can be attributed to structural interactions [88]. The high removal of BSA for the membrane was also regarded as an indication of significant protein removal, in addition to the electrostatic repulsion phenomena, owing to its structural relationship.

The investigation conducted by Shaikh et al. [89], focused on the

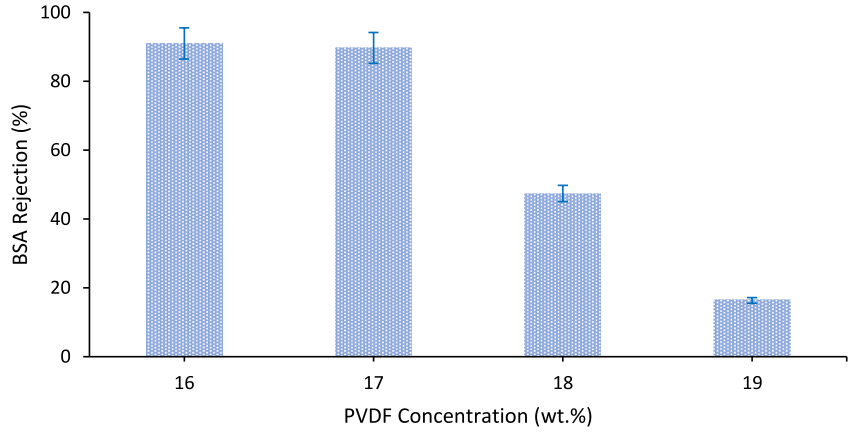

Fig. 6. BSA rejection of membranes with different PVDF concentrations.

adsorption process of bovine serum albumin (BSA) onto poly (vinylidene fluoride) (PVDF) surfaces within an aqueous environment. This investigation employed molecular dynamics simulations to examine the adsorption phenomenon in the presence and absence of excess ions. The adsorption process encompasses the diffusion of proteins towards the surface and subsequent dehydration of surface-protein contacts, leading to adsorption and denaturation. Proteins exhibit higher adsorption on hydrophobic or less hydrophilic surfaces than on hydrophilic surfaces.

The observed decline in BSA fluxes over time may be attributed to the occurrence of pore blockage in the membranes caused by the adsorption and deposition of BSA proteins on the membrane surface. This phenomenon is likely mitigated by using high molecular weight BSA molecules (66 kDa) on the membrane surface, reducing concentration polarization's impact. Moreover, it has been observed that the early decreases in flux are more pronounced, whereas the subsequent declines in flux occur gradually. This phenomenon can be attributed to the reduction in porosity of the membrane caused by the internal adsorption of BSA protein, resulting in pore blockage [84].

The synergistic impact of polyvinylpyrrolidone (PVP) and titanium dioxide has been found to substantially influence enhancing resistance to membrane fouling resulting from bovine serum albumin adsorption. This effect is attributed to the reduction of hydrophobic interactions between BSA protein molecules and the surface of the membrane. The hydrophilic nature of a surface enables it to attract and bind water molecules, forming a hydration layer. This layer plays a crucial role in impeding the adsorption of contaminants within the membrane [90]. According to Zhang et al. [91], membrane fouling mainly results from protein deposition on the surface or entrapment within the pores, leading to irreversible resistance and loose protein adsorption on the membrane surface, resulting in reversible resistance.

4. Conclusions

The hydrophile level of the membrane can be raised by combining polymeric additions of PVP and nanoparticle TiO_2 in a PVDF polymer solution. An essential factor for modifying membrane characteristics was the polymer composition of a dope solution. This study investigated the fabrication of PVDF-TiO_2-PVP membranes and assessed the effects of PVDF polymer concentration on membrane formation, final structure, and membrane characteristics. The FESEM images show that different PVDF concentrations have different effects; a 16-wt percent PVDF membrane has a thinner skin layer and more macro-voids than a 17 to 19-wt percent PVDF membrane. All PVDF-TiO_2-PVP membranes' elemental results (C, O, F, and Ti) are comparable at doses of 16–19 wt% PVDF, with only minor variations in the weight percentage of each element. The outcomes showed that TiO_2 and PVDF utilized FTIR to detect their existence. The contact angle measurements demonstrated that the hydrophilicity of membranes decreased as the amount of polymer increased. The tensile strength of the other membranes ranges from 19 wt% PVDF (2.403 KPa) to 16 wt% PVDF (1.752 KPa), with 16 wt% PVDF had the lowest tensile strength. The highest water flux (265.43 L/m^2h) and BSA flux (250.31 L/m^2h) were obtained by 19 wt% PVDF. The BSA is rejected with 91.01 % at the lowest concentration of PVDF (16 wt%) and 16.34 % at the highest concentration (19 wt%). PVDF-TiO_2-PVP membranes were shown to be a potential novel material for the purification of protein solutions in this investigation. The high-water flux and BSA rejection rate of the membranes make them ideal for this purpose.

CRediT authorship contribution statement

Rianyza Gayatri: Conceptualization, Data curation, Writing – original draft, Writing – review & editing. **Ahmad Noor Syimir Fizal:** Writing – review & editing. **Erna Yuliwati:** Conceptualization, Supervision. **Muhamad Zulhilmi Zailani:** Supervision, Writing – review & editing. **Juhana Jaafar:** Supervision, Writing – review & editing. **Md Sohrab Hossain:** Conceptualization, Supervision, Writing – review & editing. **Muzafar Zulkifli:** Conceptualization, Supervision, Writing – review & editing. **Wirach Taweepreda:** Conceptualization, Funding acquisition, Project administration, Supervision, Writing – review & editing. **Ahmad Naim Ahmad Yahaya:** Conceptualization, Funding acquisition, Project administration, Writing – review & editing.

Declaration of competing interest

The authors declare that they have no known competing financial interests or personal relationships that could have appeared to influence the work reported in this paper.

Data availability

Data will be made available on request.

Acknowledgments

The authors acknowledge Prince of Songkla Universiti and Universiti Kuala Lumpur under UERGS grant (UER20009 65458-315009) for the financial assistance provided for the publication of this manuscript.

References

[1] B. Doshi, M. Sillanpää, S. Kalliola, A review of bio-based materials for oil spill treatment, Water Res. 135 (2018) 262–277, https://doi.org/10.1016/j.watres.2018.02.034.
[2] R. Sengur-Tasdemir, G.M. Urper-Bayram, T. Turken, E. Ates-Genceli, V. V. Tarabara, I. Koyuncu, Hollow fiber nanofiltration membranes for surface water treatment: performance evaluation at the pilot scale, J. Water Proc. Eng. 42 (Aug. 2021), https://doi.org/10.1016/j.jwpe.2021.102100.
[3] H. Liu, H. Yu, X. Yuan, W. Ding, Y. Li, J. Wang, Amino-functionalized mesoporous PVA/SiO2 hybrids coated membrane for simultaneous removal of oils and water-soluble contaminants from emulsion, Chem. Eng. J. 374 (May) (2019) 1394–1402, https://doi.org/10.1016/j.cej.2019.05.161.
[4] S. Gao, X. Dong, J. Huang, S. Li, Y. Li, Z. Chen, Yuekun Lai, Rational construction of highly transparent superhydrophobic coatings based on a non-particle, fluorine-free and water-rich system for versatile oil-water separation, Chem. Eng. J. 333 (2018) 621–629, https://doi.org/10.1016/j.cej.2017.10.006.
[5] J. Wu, Y. He, L. Zhou, X. Yin, L. Zhang, J. Chen, Z. Li, Y. Bai, TiO_2@HNTs robustly decorated PVDF membrane prepared by a bioinspired accurate-deposition strategy for complex corrosive wastewater treatment, ACS Appl. Mater. Interfaces 13 (9) (2021) 11320–11331, https://doi.org/10.1021/acsami.1c00697.
[6] Q.V. Ly, C.N. Matindi, A.T. Kuvarega, Q.V. Le, V.S. Tran, Y. Hu, J. Li, Organic fouling assessment of novel PES/SPSf/Double layered hydroxide mixed matrix membrane for water treatment application, J. Water Proc. Eng. 37 (Oct) (2020), https://doi.org/10.1016/j.jwpe.2020.101526.
[7] F. Caron, S. Siemann, R. Riopel, Characterization of the natural organic matter (NOM) in groundwater contaminated with 60Co and 137Cs using ultrafiltration, solid phase extraction and fluorescence analysis, J. Environ. Radioact. 138 (2014) 331–340, https://doi.org/10.1016/j.jenvrad.2013.12.024.
[8] X. Zhao, Y. Su, J. Cao, Y. Li, R. Zhang, Y. Li, Z. Jiang, Fabrication of antifouling polymer-inorganic hybrid membranes through the synergy of biomimetic mineralization and nonsolvent induced phase separation, J. Mater. Chem. A Mater. 3 (14) (2015) 7287–7295, https://doi.org/10.1039/c5ta00654f.
[9] W. Jiao, Y. Ban, Z. Shi, X. Jiang, Y. Li, W. Yang, Gas separation performance of supported carbon molecular sieve membranes based on soluble polybenzimidazole, J. Membr. Sci. 533 (March) (2017) 1–10, https://doi.org/10.1016/j.memsci.2017.03.022.
[10] F. Salehi, Current and future applications for nanofiltration technology in the food processing, Food Bioprod. Process. 92 (2) (2014) 161–177, https://doi.org/10.1016/j.fbp.2013.09.005.
[11] M. Rabiller-Baudry, A. Bouzin, C. Hallery, J. Girard, C. Leperoux, Evidencing the chemical degradation of a hydrophilised PES ultrafiltration membrane despite protein fouling, Sep. Purif. Technol. 147 (2015) 62–81, https://doi.org/10.1016/j.seppur.2015.03.056.
[12] N. Arahman, Syawaliah Mukramah, T. Maimun, M.R. Bilad, Fabrication of polyethersulfone membranes using nanocarbon as additive, Int. J. GEOMATE 15 (50) (2018) 51–57, https://doi.org/10.21660/2018.50.95424.
[13] R. Singh, V. Volli, L. Lohani, M.K. Purkait, Polymeric ultrafiltration membranes modified with fly ash-based carbon nanotubes for thermal stability and protein separation, Case Stud. Chem. Environ. Eng. 4 (Dec) (2021), https://doi.org/10.1016/j.cscee.2021.100155.
[14] T.D. Kusworo, N. Ariyanti, D.P. Utomo, Effect of nano-TiO_2 loading in polysulfone membranes on the removal of pollutant following natural-rubber wastewater treatment, J. Water Proc. Eng. 35 (Jun. 2020), https://doi.org/10.1016/j.jwpe.2020.101190.

[15] E.J. Lee, A.K. An, T. He, Y.C. Woo, H.K. Shon, Electrospun nanofiber membranes incorporating fluorosilane-coated TiO2 nanocomposite for direct contact membrane distillation, J. Membr. Sci. 520 (2016) 145–154, https://doi.org/10.1016/j.memsci.2016.07.019.

[16] D. Attarde, M. Jain, P.K. Singh, S.K. Gupta, Energy-efficient seawater desalination and wastewater treatment using osmotically driven membrane processes, Desalination 413 (2017) 86–100, https://doi.org/10.1016/j.desal.2017.03.010.

[17] J. Zhang, Z. Wang, Q. Wang, C. Pan, Z. Wu, Comparison of antifouling behaviours of modified PVDF membranes by TiO2 sols with different nanoparticle size: implications of casting solution stability, J. Membr. Sci. 525 (July 2016) (2017) 378–386, https://doi.org/10.1016/j.memsci.2016.12.021.

[18] M. Chai, Y. Ye, V. Chen, Separation and concentration of milk proteins with a submerged membrane vibrational system, J. Membr. Sci. 524 (November 2016) (2017) 305–314, https://doi.org/10.1016/j.memsci.2016.11.043.

[19] R. Gayatri, et al., Preparation and characterization of PVDF–TiO_2 mixed-matrix membrane with PVP and PEG as pore-forming agents for BSA rejection, Nanomaterials 13 (6) (2023) 1023, https://doi.org/10.3390/nano13061023.

[20] D. Li, X. Sun, C. Gao, M. Dong, Improved water flux and antifouling properties of cardo poly(aryl ether ketone) ultrafiltration membrane by novel sulfobetaine polyimides additive, Sep. Purif. Technol. 251 (2020) 117144, https://doi.org/10.1016/j.seppur.2020.117144.

[21] A.M. Abu-dief, S. Bin, O. Alzahrani, Int. J. Organic Inorganic Chem. Rev. Article Sustain. Nanocomposites Water Treatment (February) (2020).

[22] N. Bazrafshan, M. Dadashi Firouzjaei, M. Elliott, A. Moradkhani, A. Rahimpour, Preparation and modification of low-fouling ultrafiltration membranes for cheese whey treatment by membrane bioreactor, Case Stud. Chem. Environ. Eng. 4 (Dec. 2021), https://doi.org/10.1016/j.cscee.2021.100137.

[23] A.M. Abu-Dief, S. Kamel Hamdan, Functionalization of magnetic nano particles: synthesis, characterization and their application in water purification, American J. Nanosci. 2 (3) (2016) 26–40, https://doi.org/10.11648/j.ajn.20160203.12.

[24] G.P.S. Ibrahim, A.M. Isloor, A.M. Asiri, N. Ismail, Novel, one-step synthesis of zwitterionic polymer nanoparticles polymerization and its application for dye removal membrane, Sci. Rep. 7 (July) (2017) 1–16, https://doi.org/10.1038/s41598-017-16131-9.

[25] C. T-Rodríguez, J. C-García, L. T-Sánchez, A.L.A.M. Abu-Dief, A. Costa, L. Elbaile, R.D. Crespo, J.S. Garitaonandia, E. Lastra, J.A. García, F.J. G-Alonso, A simple and reliable synthesis of superparamagnetic magnetite nanoparticles by thermal decomposition of $Fe(acac)_3$, J. Nanomater. 2019 (2019), https://doi.org/10.1155/2019/2464010.

[26] W.S. Mohamed, M. Alzaid, M.S.M. Abdelbaky, Z. Amghouz, Impact of Co^{2+} substitution on microstructure and magnetic properties of Co_xZn_{1-x} Fe_2O_4 nanoparticles, Nanomaterials 9 (11) (2019) 1602.

[27] E.A. Genceli, R. S-Tasdemir, G.M. Urper, S. Gumrukcu, Z. G-Gokce, U. Dagli, T. Turken, A.S. Sarac, Koyuncu Ismail, Effects of carboxylated multi-walled carbon nanotubes having different outer diameters on hollow fiber ultrafiltration membrane fabrication and characterization by electrochemical impedance spectroscopy, Polym. Bull. 75 (6) (2018) 2431–2457, https://doi.org/10.1007/s00289-017-2155-3.

[28] M. Tian, R. Wang, A. Goto, W. Mao, Y. Miyoshi, H. Mizoguchi, Performance enhancement of ultrafiltration membrane via simple deposition of polymer-based modifiers, J. Water Proc. Eng. 33 (Feb. 2020), https://doi.org/10.1016/j.jwpe.2019.101034.

[29] D.T. Tran, J.P. Méricq, J. Mendret, S. Brosillon, C. Faur, Influence of preparation temperature on the properties and performance of composite PVDF-TiO_2 membranes, Membranes 11 (11) (2021), https://doi.org/10.3390/membranes11110876.

[30] S. Lustenberger, R. Castro-Muñoz, Advanced biomaterials and alternatives tailored as membranes for water treatment and the latest innovative European water remediation projects: a review, Case Stud. Chem. Environ. Eng. 5 (May 2022), https://doi.org/10.1016/j.cscee.2022.100205.

[31] M. Safarpour, A. Khataee, V. Vatanpour, Thin film nanocomposite reverse osmosis membrane modified by reduced graphene oxide/TiO_2 with improved desalination performance, J. Membr. Sci. 489 (2015) 43–54, https://doi.org/10.1016/j.memsci.2015.04.010.

[32] J. Zhang, M. Zheng, Y. Zhou, L. Yang, Y. Zhang, Z. Wu, G. Liu, Junjian Zheng, Preparation of nano-TiO_2-modified PVDF membranes with enhanced antifouling behaviors via phase inversion: implications of nanoparticle dispersion status in casting solutions, Membranes 12 (4) (2022) 1–17, https://doi.org/10.3390/membranes12040386.

[33] S. Leong, A. Razmjou, K. Wang, K. Hapgood, X. Zhang, H. Wang, TiO_2 based photocatalytic membranes: a review, J. Membr. Sci. 472 (2014) 167–184, https://doi.org/10.1016/j.memsci.2014.08.016.

[34] H. Basri, A.F. Ismail, M. Aziz, Polyethersulfone (PES)-silver composite UF membrane: effect of silver loading and PVP molecular weight on membrane morphology and antibacterial activity, Desalination 273 (1) (2011) 72–80, https://doi.org/10.1016/j.desal.2010.11.010.

[35] W.Z. Lang, J.P. Shen, Y.T. Wei, Q.Y. Wu, J. Wang, Y.J. Guo, Precipitation kinetics, morphologies, and properties of poly(vinyl butyral) hollow fiber ultrafiltration membranes with respect to polyvinylpyrrolidone molecular weight, Chem. Eng. J. 225 (2013) 25–33, https://doi.org/10.1016/j.cej.2013.03.061.

[36] M. Sadrzadeh, S. Bhattacharjee, Rational design of phase inversion membranes by tailoring thermodynamics and kinetics of casting solution using polymer additives, J. Membr. Sci. 441 (2013) 31–44, https://doi.org/10.1016/j.memsci.2013.04.009.

[37] P.S. Goh, B.C. Ng, W.J. Lau, A.F. Ismail, Inorganic nanomaterials in polymeric ultrafiltration membranes for water treatment, Separ. Purif. Rev. 44 (3) (2015) 216–249, https://doi.org/10.1080/15422119.2014.926274.

[38] J.H. Li, X.S. Shao, Q. Zhou, M.Z. Li, Q.Q. Zhang, The double effects of silver nanoparticles on the PVDF membrane: surface hydrophilicity and antifouling performance, Appl. Surf. Sci. 265 (2013) 663–670, https://doi.org/10.1016/j.apsusc.2012.11.072.

[39] N. Akther, S. Phuntsho, Y. Chen, N. Ghaffour, H.K. Shon, Recent advances in nanomaterial-modified polyamide thin-film composite membranes for forward osmosis processes, J. Membr. Sci. 584 (2019) 20–45, https://doi.org/10.1016/j.memsci.2019.04.064.

[40] D. Emadzadeh, W.J. Lau, T. Matsuura, A.F. Ismail, M. Rahbari-Sisakht, Synthesis and characterization of thin film nanocomposite forward osmosis membrane with hydrophilic nanocomposite support to reduce internal concentration polarization, J. Membr. Sci. 449 (2014) 74–85, https://doi.org/10.1016/j.memsci.2013.08.014.

[41] J.P. Méricq, J. Mendret, S. Brosillon, C. Faur, High performance PVDF-TiO_2 membranes for water treatment, Chem. Eng. Sci. 123 (2015) 283–291, https://doi.org/10.1016/j.ces.2014.10.047.

[42] A. Soroush, W. Ma, Y. Silvino, M.S. Rahaman, Surface modification of thin film composite forward osmosis membrane by silver-decorated graphene-oxide nanosheets, Environ. Sci.: Nano 2 (4) (2015) 395–405, https://doi.org/10.1039/c5en00086f.

[43] N. Ma, J. Wei, R. Liao, C.Y. Tang, Zeolite-polyamide thin film nanocomposite membranes: towards enhanced performance for forward osmosis, J. Membr. Sci. 405 (406) (2012) 149–157, https://doi.org/10.1016/j.memsci.2012.03.002.

[44] S. Hamzah, N. Ali, M.M. Ariffin, A. Ali, A.W. Mohammad, High performance of polysulfone ultrafiltration membrane: effect of polymer concentration, ARPN J. Eng. Appl. Sci. 9 (12) (2014) 2543–2550.

[45] H. Julian, Polysulfone membranes for CO_2/CH_4 separation: state of the art, IOSR J. Eng. 2 (3) (2012) 484–495, https://doi.org/10.9790/3021-0203484495.

[46] N.M. Ismail, N.R. Jakariah, N. Bolong, S.M. Anissuzaman, N.A.H.M. Nordin, A. R. Razali, Effect of polymer concentration on the morphology and mechanical properties of asymmetric polysulfone (PSf) membrane, J. Appl. Membrane Sci. & Technol. 21 (1) (2017) 33–41, https://doi.org/10.11113/amst.v21i1.107.

[47] M.A.U.R. Alvi, M.A. Khalid, N.M. Ahmad, M.B.K. Niazi, M.N. Anwar, M. Batool, W. Cheema, S. Rafiq, Polymer concentration and solvent variation correlation with the morphology and water filtration analysis of polyether sulfone microfiltration membrane, Adv. Polym. Technol. 2019 (2019), https://doi.org/10.1155/2019/8074626.

[48] C.Y. Lai, A. Groth, S. Gray, M. Duke, Impact of casting conditions on PVDF/nanoclay nanocomposite membrane properties, Chem. Eng. J. 267 (2015) 73–85, https://doi.org/10.1016/j.cej.2014.12.036.

[49] M.H.D.A. Farahani, V. Vatanpour, A comprehensive study on the performance and antifouling enhancement of the PVDF mixed matrix membranes by embedding different nanoparticulates: clay, functionalized carbon nanotube, SiO_2 and TiO_2, Sep. Purif. Technol. 197 (October 2017) (2018) 372–381, https://doi.org/10.1016/j.seppur.2018.01.031.

[50] Y. Feng, G. Han, T.S. Chung, M. Weber, N. Widjojo, C. Maletzko, Effects of polyethylene glycol on membrane formation and properties of hydrophilic sulfonated polyphenylenesulfone (sPPSU) membranes, J. Membr. Sci. 531 (February) (2017) 27–35, https://doi.org/10.1016/j.memsci.2017.02.040.

[51] N. Nabian, A.A. Ghoreyshi, A. Rahimpour, M. Shakeri, Effect of polymer concentration on the structure and performance of PEI hollow fiber membrane contactor for CO_2 stripping, J. Hazard Mater. 250–251 (2) (2013) 354–361, https://doi.org/10.1016/j.jhazmat.2013.01.083.

[52] N. Nabian, A.A. Ghoreyshi, A. Rahimpour, M. Shakeri, Effect of polymer concentration on the structure and performance of PEI hollow fiber membrane contactor for CO_2 stripping, J. Hazard Mater. 250–251 (2) (2013) 354–361, https://doi.org/10.1016/j.jhazmat.2013.01.083.

[53] R. Naim, A.F. Ismail, A. Mansourizadeh, Effect of non-solvent additives on the structure and performance of PVDF hollow fiber membrane contactor for CO_2 stripping, J. Membr. Sci. 423 (424) (2012) 503–513, https://doi.org/10.1016/j.memsci.2012.08.052.

[54] A.L. Ahmad, T.A. Otitoju, B.S. Ooi, Hollow fiber (HF) membrane fabrication: a review on the effects of solution spinning conditions on morphology and performance, J. Ind. Eng. Chem. 70 (2019) 35–50, https://doi.org/10.1016/j.jiec.2018.10.005.

[55] H. Li, W. Shi, X. Zeng, S. Huang, H. Zhang, X. Qin, Improved desalination properties of hydrophobic GO-incorporated PVDF electrospun nanofibrous composites for vacuum membrane distillation, Sep. Purif. Technol. 230 (February 2019) (2020) 115889, https://doi.org/10.1016/j.seppur.2019.115889.

[56] D. Matveev, I. Borisov, V. Vasilevsky, G. Karpacheva, V. Volkov, Spinning of polysulfone hollow fiber membranes using constant dope solution composition: viscosity control via temperature, Membranes 12 (12) (2022), https://doi.org/10.3390/membranes12121257.

[57] D. Rana, K. Bag, S.N. Bhattacharyya, B.M. Mandal, Miscibility of poly(styrene-co-butyl acrylate) with poly(ethyl methacrylate): existence of both UCST and LCST, J. Polym. Sci., Part B: Polym. Phys. 38 (2000) 369–375, https://doi.org/10.1002/(SICI)1099-0488(20000201)38:3<369::AID-POLB3>3.0.CO;2-W.

[58] D. Rana, B.M. Mandal, S.N. Bhattacharyya, Analogue calorimetric studies of blends of poly(vinyl ester)s and polyacrylates, Macromolecules 29 (No. 5) (1996) 1579–1583, 0024-9297/96/2229-1579$12.00/0.

[59] D. Rana, B.M. Mandal, S.N. Bhattacharyya, Analogue calorimetry of polymer blends: poly(styrene-co-acrylonitrile) and poly(phenyl acrylate) or poly(vinyl benzoate), Polymer 37 (12) (1996) 2439–2443, https://doi.org/10.1016/0032-3861(96)85356-0.

[60] D. Rana, B.M. Mandal, S.N. Bhattacharyya, Miscibility and phase diagrams of poly (phenyl acrylate) and poly (styrene-co-acrylonitrile) blends, Polymer 34 (7) (1993), 1993. 0032-3861/93/071454-06.

[61] C.S. Ong, W.J. Lau, P.S. Goh, B.C. Ng, A.F. Ismail, Preparation and characterization of PVDF–PVP–TiO_2 composite hollow fiber membranes for oily wastewater treatment using submerged membrane system, Desalination Water Treat. 53 (5) (2013) 1213–1223, https://doi.org/10.1080/19443994.2013.855679.
[62] M.U. Abba, H.C. Man, R.S. Azis, M.H. Hamzah, A.I. Idris, K.F. Yunos, K.K. Katibi, Novel PVDF-PVP hollow fiber membrane augmented with TiO_2 nanoparticles: preparation, characterization and application for copper removal from leachate, Nanomaterials 11 (2) (Feb. 2021) 1–18, https://doi.org/10.3390/nano11020399.
[63] C.S. Ong, W.J. Lau, P.S. Goh, A.F. Ismail, Preparation and characterization of PVDF-TiO_2 composite membranes blended with different Mw of PVP for oily wastewater treatment using submerged membrane system, Jurnal Teknologi (Sci. Eng.) 69 (9) (2014) 53–56, https://doi.org/10.11113/jt.v69.3396.
[64] B. Zhou. Simulations of Polymeric Membrane Formation in 2D and 3D, Massachusetts Institute of Technology, 2006, p. 213.
[65] H. Sofiah, A. Nora'aini, M.A. Marinah, The influence of polymer concentration on performance and morphology of asymmetric ultrafiltration membrane for lysozyme separation, J. Appl. Sci. 10 (24) (2010) 3325–3330, https://doi.org/10.3923/jas.2010.3325.3330.
[66] A. Abdullah, P. Peechmani, M. Hafiz, D. Othman, M. Hafiz, Removal of organic dye in wastewater using polyethersulfone hollow fiber membrane, Appl. Membrane Sci.; Technol. 26 (2) (2022) 29–42.
[67] U.N. Rusli, N.H. Alias, M.Z. Shahruddin, N.H. Othman, Photocatalytic degradation of oil using polyvinylidene fluoride/titanium dioxide composite membrane for oily wastewater treatment, MATEC Web Conf. 69 (2016), https://doi.org/10.1051/matecconf/20166905003.
[68] Q. Zhang, X. Lu, Q. Zhang, L. Zhang, S. Li, S. Liu, Flux and passage enhancement in hemodialysis by incorporating compound additive into PVDF polymer matrix, Membranes 6 (4) (2016) 1–16, https://doi.org/10.3390/membranes6040045.
[69] Q. Zhang, X. Lu, L. Zhao, Preparation of polyvinylidene fluoride (PVDF) hollow fiber hemodialysis membranes, Membranes 4 (1) (2014) 81–95, https://doi.org/10.3390/membranes4010081.
[70] M. Abdennouri, et al., Photocatalytic degradation of 2,4-D and 2,4-DP herbicides on Pt/TiO_2 nanoparticles, J. Saudi Chem. Soc. 19 (5) (Sep. 2015) 485–493, https://doi.org/10.1016/j.jscs.2015.06.007.
[71] A. Fadaei, A. Salimi, M. Mirzataheri, Structural elucidation of morphology and performance of the PVDF/PEG membrane, J. Polym. Res. 21 (9) (2014), https://doi.org/10.1007/s10965-014-0545-x.
[72] C. Du, Z. Wang, G. Liu, W. Wang, D. Yu, One-step electrospinning PVDF/PVP-TiO_2 hydrophilic nanofiber membrane with strong oil-water separation and anti-fouling property, Colloids Surf. A Physicochem. Eng. Asp. 624 (May) (2021) 126790, https://doi.org/10.1016/j.colsurfa.2021.126790.
[73] R. Naim, A.F. Ismail, Effect of polymer concentration on the structure and performance of PEI hollow fiber membrane contactor for CO_2 stripping, J. Hazard Mater. 250 (251) (2013) 354–361, https://doi.org/10.1016/j.jhazmat.2013.01.083.
[74] E. Pramono, A.L. Simamora, C.L. Radiman, D. Wahyuningrum, Effects of PVDF concentration on the properties of PVDF membranes, IOP Conf. Ser. Earth Environ. Sci. 75 (1) (2017), https://doi.org/10.1088/1755-1315/75/1/012027.
[75] T.N. Baroud, Tuning PVDF membrane porosity and wettability resistance via varying substrate morphology for the desalination of highly saline water, Membranes 13 (4) (2023), https://doi.org/10.3390/membranes13040395.
[76] J.A. Kharraz, A.K. An, Patterned superhydrophobic polyvinylidene fluoride (PVDF) membranes for membrane distillation: enhanced flux with improved fouling and wetting resistance, J. Membr. Sci. 595 (2020) 117596, https://doi.org/10.1016/j.memsci.2019.117596.
[77] C.Y. Lai, A. Groth, S. Gray, M. Duke, Impact of casting conditions on PVDF/nanoclay nanocomposite membrane properties, Chem. Eng. J. 267 (2015) 73–85, https://doi.org/10.1016/j.cej.2014.12.036.
[78] G. Li, W. Kujawski, K. Knozowska, J. Kujawa, The effects of PEI hollow fiber substrate characteristics on PDMS/PEI hollow fiber membranes for CO_2/N_2 separation, Membranes 11 (1) (2021) 1–23, https://doi.org/10.3390/membranes11010056.
[79] D. Rana, H.L. Kim, H. Kwag, S. Choe, Hybrid blends of similar ethylene 1-octene copolymers, Polymer 41 (2000) 7067–7082.
[80] D. Rana, K. Cho, T. Woo, B.H. Lee, S. Choe, Blends of ethylene 1-octene copolymer synthesized by ziegler-natta and metallocene catalysts. I. Thermal and mechanical properties, J. Appl. Polym. Sci. 74 (1999) 1169–1177.
[81] D. Rana, et al., Blends of ethylene 1-octene copolymer synthesized by ziegler-natta and metallocene catalysts. II. Rheology and morphological behaviors, J. Appl. Polym. Sci. 76 (2000) 1950–1964.
[82] D. Rana, C.H. Lee, K. Cho, B.H. Lee, S. Choe, Thermal and mechanical properties for binary blends of metallocene polyethylene with conventional polyolefins, J. Appl. Polym. Sci. 69 (1998) 2441–2450. John Wiley & Sons, Inc.
[83] C. Dong, G. He, H. Li, R. Zhao, Y. Han, Y. Deng, Antifouling enhancement of poly (vinylidene fluoride) microfiltration membrane by adding $Mg(OH)_2$ nanoparticles, J. Membr. Sci. 387–388 (1) (2012) 40–47, https://doi.org/10.1016/j.memsci.2011.10.007.
[84] K.A. Gebru, C. Das, Removal of bovine serum albumin from wastewater using fouling resistant ultrafiltration membranes based on the blends of cellulose acetate, and PVP-TiO2 nanoparticles, J. Environ. Manag. 200 (Sep. 2017) 283–294, https://doi.org/10.1016/j.jenvman.2017.05.086.
[85] T. Wu, B. Zhou, T. Zhu, J. Shi, Z. Xu, C. Hua, J. Wang, Facile and low-cost approach towards a PVDF ultrafiltration membrane with enhanced hydrophilicity and antifouling performance via graphene oxide/water-bath coagulation, RSC Adv. 5 (11) (2015) 7880–7889, https://doi.org/10.1039/c4ra13476a.
[86] M. Kumar, Z. Gholamvand, A. Morrissey, K. Nolan, M. Ulbricht, J. Lawler, Preparation and characterization of low fouling novel hybrid ultrafiltration membranes based on the blends of GO-TiO_2 nanocomposite and polysulfone for humic acid removal, J. Membr. Sci. 506 (May 2016) 38–49, https://doi.org/10.1016/j.memsci.2016.02.005.
[87] H. Mo, K.G. Tay, H.Y. Ng, Fouling of reverse osmosis membrane by protein (BSA): effects of pH, calcium, magnesium, ionic strength and temperature, J. Membr. Sci. 315 (1–2) (May 2008) 28–35, https://doi.org/10.1016/j.memsci.2008.02.002.
[88] X. Cao, J. Ma, X. Shi, Z. Ren, Effect of TiO_2 nanoparticle size on the performance of PVDF membrane, Appl. Surf. Sci. 253 (4) (Dec. 2006) 2003–2010, https://doi.org/10.1016/j.apsusc.2006.03.090.
[89] A.R. Shaikh, H. Karkhanechi, T. Yoshioka, H. Matsuyama, H. Takaba, D.M. Wang, Adsorption of bovine serum albumin on poly(vinylidene fluoride) surfaces in the presence of ions: a molecular dynamics simulation, J. Phys. Chem. B 122 (6) (Feb. 2018) 1919–1928, https://doi.org/10.1021/acs.jpcb.7b10221.
[90] S. Zinadini, A.A. Zinatizadeh, M. Rahimi, V. Vatanpour, H. Zangeneh, Preparation of a novel antifouling mixed matrix PES membrane by embedding graphene oxide nanoplates, J. Membr. Sci. 453 (Mar. 2014) 292–301, https://doi.org/10.1016/j.memsci.2013.10.070.
[91] J. Zhang, Z. Xu, W. Mai, C. Min, B. Zhou, M. Shan, Y. Li, C. Yang, Z. Wang, X. Qian, Improved hydrophilicity, permeability, antifouling and mechanical performance of PVDF composite ultrafiltration membranes tailored by oxidized low-dimensional carbon nanomaterials, J. Mater. Chem. A Mater. 1 (9) (Mar. 2013) 3101–3111, https://doi.org/10.1039/c2ta01415g.